

OBSERVATION OF DOPPLER BROADENING IN  $\beta$ -DELAYED PROTON- $\gamma$  DECAY

By

Sarah Schwartz

A THESIS

Submitted to

Michigan State University

in partial fulfillment of the requirements

for the degree of

Master of Science in Physics

2016

## ABSTRACT

# OBSERVATION OF DOPPLER BROADENING IN $\beta$ -DELAYED PROTON- $\gamma$ DECAY

By

**Sarah Schwartz**

The Doppler broadening of  $\gamma$ -ray peaks due to nuclear recoil from  $\beta$ -delayed nucleon emission can be used to measure the energies of the nucleons. The purpose of this Thesis is to test and apply this Doppler broadening method using  $\gamma$ -ray peaks from the  $^{26}\text{P}(\beta\text{p}\gamma)^{25}\text{Al}$  decay sequence. A fast beam of  $^{26}\text{P}$  was implanted into a planar Ge detector, which was used as a  $^{26}\text{P}$   $\beta$ -decay trigger. The SeGA array of high-purity Ge detectors was used to detect  $\gamma$  rays from the  $^{26}\text{P}(\beta\text{p}\gamma)^{25}\text{Al}$  decay sequence. Radiative Doppler broadening in  $\beta$ -delayed proton- $\gamma$  decay was observed for the first time. The Doppler broadening analysis method was verified using the 1613 keV  $\gamma$ -ray line for which the proton energies were previously known. The 1776 keV  $\gamma$  ray de-exciting the 2720 keV  $^{25}\text{Al}$  level was observed in  $^{26}\text{P}(\beta\text{p}\gamma)^{25}\text{Al}$  decay for the first time and used to determine that the center-of-mass energy of the proton emission feeding the 2720-keV level is  $5.1 \pm 1.0$  (*stat.*)  $\pm 0.6$  (*syst.*) MeV, corresponding to a  $^{26}\text{Si}$  excitation energy of  $13.3 \pm 1.0$  (*stat.*)  $\pm 0.7$  (*syst.*) MeV for the proton-emitting level. The Doppler broadening method has been demonstrated to provide practical measurements of the energies for  $\beta$ -delayed nucleon emissions populating excited states of nuclear recoils at least as heavy as  $A = 25$ .

# TABLE OF CONTENTS

<b>Chapter 1</b>	<b>Introduction</b>	<b>1</b>
1.1	Introduction to the nucleus	1
1.2	Types of nuclear decay	1
1.3	Beta-Delayed Nucleon Emission	2
1.4	Previous work in Doppler broadening of $\beta$ delayed nucleon- $\gamma$ decay	5
1.5	Example of Doppler broadening analysis	5
<b>Chapter 2</b>	<b>Experiment</b>	<b>8</b>
2.1	Lab Layout	8
2.2	Detectors	9
<b>Chapter 3</b>	<b>Data Analysis and Discussion</b>	<b>13</b>
3.1	Gamma-ray Intensities	13
3.2	$\beta p$ Feeding	16
3.3	Study of Doppler Broadened Peaks	17
3.4	1613 keV	23
3.5	1776 keV	26
<b>Chapter 4</b>	<b>Conclusion and outlook</b>	<b>29</b>

# Chapter 1

## Introduction

### 1.1 Introduction to the nucleus

The atom is a building block of all matter. It is neutral and composed mostly of empty space. Essentially all of its mass concentrated in the positively charged nucleus while the remainder of its mass is in the negatively charged electrons which surround the nucleus. The nucleus is composed of two different particles, the proton and the neutron. The proton is a fermion consisting of two up quarks and a down quark, giving it one positive elementary charge. The neutron is a fermion consisting of two down quarks and an up quark which results in a neutral charge. Both of these nucleons are about the same mass. It is basic knowledge that, due to the electromagnetic force, like charges repel while opposite charges attract. Even though a nucleus consists of only positive and neutral particles they are bound due to the fundamental force known as the strong nuclear force allowing them to be long-lived.

### 1.2 Types of nuclear decay

Nuclei tend to seek more energetically stable configurations by undergoing several types of nuclear decays. A few of the different types of decays include  $\alpha$ ,  $\beta$  and  $\gamma$  decay. Alpha decay refers to the spontaneous emission of an  $\alpha$  particle. Alpha decay is mediated by a combination of the attractive strong force and the repulsive electromagnetic force. There

are similar decays in which only one nucleon (a neutron or a proton) is emitted. These are neutron and proton emission, named after the nucleon that was emitted, often from excited states. The next fundamental decay is  $\beta$  decay, which is the emission of a  $\beta$  particle mediated by the weak nuclear force. There are two types of  $\beta$  decays,  $\beta^-$  and  $\beta^+$ . In  $\beta^-$  decay a neutron decays into a proton,  $\beta^-$  particle (electron) and electron anti-neutrino. In  $\beta^+$  decay a proton decays into a neutron,  $\beta^+$  particle (positron) and electron neutrino. Finally,  $\gamma$  decay is an electromagnetic transition of a nucleus in an excited state to a lower lying state with the same number of protons and neutrons. A  $\gamma$  ray, or high energy photon, is emitted during this transition.

These decays sometimes occur in a sequence, as in the case of beta-delayed proton-gamma decay. First a parent nucleus beta decays. Then an excited state of the daughter nucleus emits a proton. Finally the granddaughter nucleus de-excites via gamma decay. The decay occurs as follows  $X_Z^A \rightarrow Y_{Z-1}^{*A} \rightarrow W_{Z-2}^{*A-1} \rightarrow W_{Z-2}^{A-1}$  where  $A$  is the atomic number,  $Z$  is the proton number,  $W$ ,  $X$ , and  $Y$  are the nucleus names, and the asterisk denotes excited states.

### 1.3 Beta-Delayed Nucleon Emission

When a nucleon is emitted from a nucleus the daughter nucleus recoils. For a given decay, if the Center of Mass (CM) energy,  $E_{CM}$ , is known then the velocity of the recoiling daughter nucleus can be calculated by employing conservation of energy and momentum.

$$\frac{1}{2}m_n v_n^2 + \frac{1}{2}m_d v_d^2 = E_{CM} \quad (1.1)$$

$$m_n v_n = -m_d v_d \quad (1.2)$$

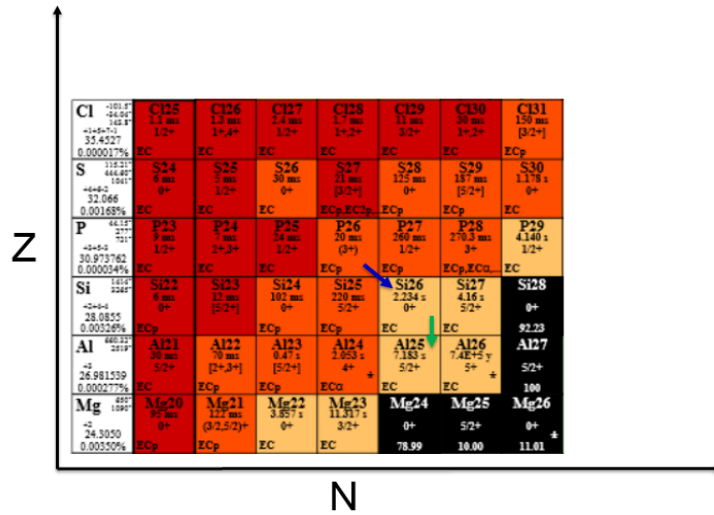


Figure 1.1: An example of  $\beta$  delayed proton emission is  $^{26}\text{P}(\beta p\gamma)^{25}\text{Al}$ . Above is a section of the chart of nuclides [6] where the number of protons,  $Z$ , is on the Y-axis and the number of neutrons,  $N$ , is on the X-axis. The blue arrow represents the  $\beta^+$  decay from  $^{26}\text{P}$  to  $^{26}\text{Si}$  which is then followed by the green arrow which represents the emission of a proton from  $^{26}\text{Si}$  to  $^{25}\text{Al}$ .

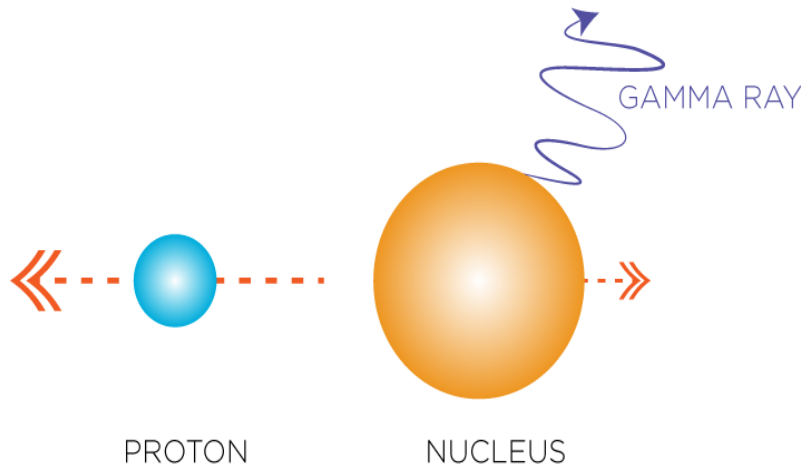


Figure 1.2:  $\beta$ -delayed proton- $\gamma$  decay is a sequence of decays in which a parent nucleus  $\beta$ -decays to become the system shown above. Next the proton is emitted causing the nucleus above to recoil. Lastly a  $\gamma$  ray is emitted in an arbitrary direction with respect to the surrounding  $\gamma$ -ray detectors, which results in a broadened peak in the  $\gamma$ -ray spectrum that is centered on the unshifted energy. Figure courtesy of Erin O'Donnell

where  $m_n$  and  $m_d$  are the mass of the nucleon and daughter nucleus, respectively, and likewise  $v_n$  and  $v_d$  are the velocities of the nucleon and daughter nucleus, respectively. Simplifying, the velocity of the daughter nucleus can be written as

$$v_d = \frac{m_n}{m_d} v_n \quad (1.3)$$

The daughter nucleus can be left in an excited state by the decay and can then de-excite via  $\gamma$  decay. If the initial velocity is high enough and the life time of the excited state is short enough then the  $\gamma$  ray will be emitted while the nucleus is still recoiling resulting in the Doppler shift of the  $\gamma$ -ray-energy in the laboratory frame. When many of these decays occur the resulting line in the  $\gamma$  ray spectrum will be Doppler broadened due to the isotropic emission of the nucleons and of the  $\gamma$  rays from the daughter nucleus.

This also allows us to find the CM energy for nucleon emission decays that are unknown. By modeling the broadening of the peak the velocity of the recoiling nucleus can be calculated and ultimately the CM energy.

However in many cases the daughter nucleus is not in a vacuum and the medium it is in has some stopping power that reduces the velocity. The velocity found via the broadening is therefore lower than the initial velocity right after the decay. Naively assuming that the initial and observed velocities of the daughter nucleus are the same results in the underestimation of the CM energy.

This can be remedied by using Bethe's stopping power equation which is incorporated in software like Stopping Power and Range of Ions in Material (SRIM) [20]. The stopping power of a material is dependent on the energy of the ion in the material. Since the ion is constantly losing energy in the material the stopping power is also constantly changing for

the nucleus traversing it.

## 1.4 Previous work in Doppler broadening of $\beta$ delayed nucleon- $\gamma$ decay

Doppler broadening of this kind has been observed from only one decay channel:  $\beta$  delayed nucleon emission from the  $^{11}\text{Li}(\beta n\gamma)^{10}\text{Be}$  decay channel [3, 10, 11, 16, 14]. The broadening of these peaks was relatively clear since the recoiling nucleus,  $^{10}\text{Be}$ , is a light nucleus allowing the CM energy from neutron emission to give  $^{10}\text{Be}$  a relatively large recoil velocity. There were four broadened peaks observed in coincidence with neutrons from this decay at 2590, 2895, 3368 and 6263 keV. These peaks were clearly broadened in relation to other peaks in the  $\gamma$  ray spectrum as can be seen in Figure 1.3. These peaks were observed to be broadened in  $\gamma$ - $\gamma$  coincidence spectra as well.

Further detail of the analysis of the  $^{11}\text{Li}(\beta n\gamma)^{10}\text{Be}$  decay and for Doppler broadening from  $\beta$  delayed nucleon emission in general were given in a paper by Fynbo in 2003 [10]. This paper described the reason for the appearance of the line shapes in relation to the half-life of the excited state and how information can be extracted from these broad peaks.

## 1.5 Example of Doppler broadening analysis

The ideal case for studying the Doppler broadening of a  $\gamma$ -ray peak from  $\beta$ -delayed nucleon- $\gamma$  decay is when a single state in the parent nucleus emits a nucleon to feed a state in the daughter nucleus. Ideally there are also no higher lying states in the daughter nucleus feeding the state of interest via  $\gamma$  decay. Furthermore, the decay occurs in vacuum and therefore it

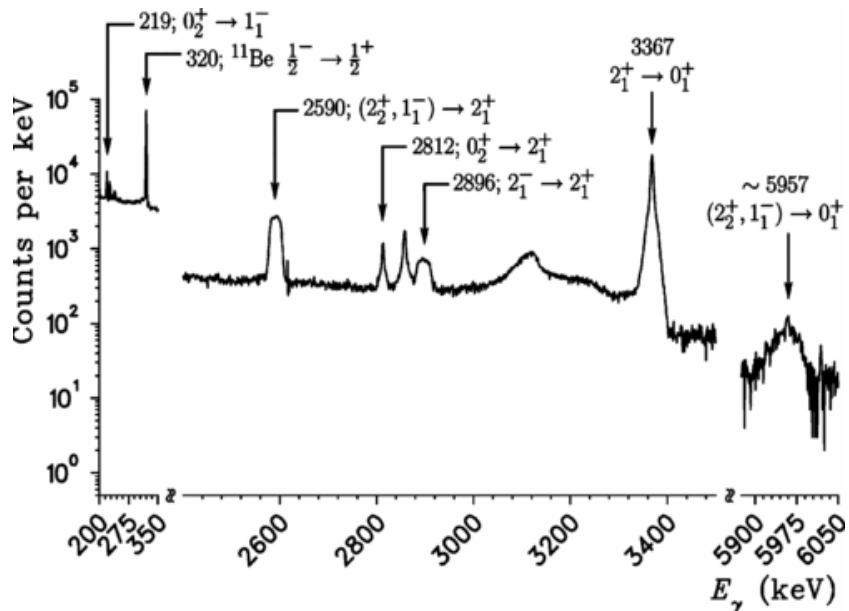


Figure 1.3: Spectrum from  $^{11}\text{Li}$   $\beta$  decay which includes broadened peaks from  $^{11}\text{Li}(\beta p \gamma)^{10}\text{Be}$  from Sarazin *et al* [16].

is not necessary to incorporate the half-life of the decaying state. Then one can convolute the detector response function with the underlying physical broadening by constructing a function of identical detector response functions spaced evenly and centered at the non-shifted energy in order to model the peak shape. This means the function used to describe the broadened peaks is the detector's response function spread out with a boxcar function.

To find how broad the peak is, the distance from the center of the highest (or lowest) energy response function to the center of the central response function can be determined. Then both of these energies would be used in a Doppler shift equation for energy where the central energy of the center peak would be called  $E_0$ , or the unshifted energy, and the center energy of the maximum peak is  $E'$ , or the shifted energy.

$$E_0 = \frac{E'c}{c + v_n} \quad (1.4)$$

where  $c$  is the speed of light and  $v_n$  is the velocity of the nucleus at the time of  $\gamma$  decay.

Now the velocity of the nucleus at the time of  $\gamma$  decay can be found. If the recoil and  $\gamma$  decay of the nucleus had occurred in free space conservation laws could be applied at this point to find the kinetic energy of the nucleon at the time of its emission and finally add it to the kinetic energy of the recoiling nucleus to find the CM energy of the decay. Unfortunately the situation is usually not so simple.

When the recoil occurs in a material, both the stopping power of the material and the half life of the excited state of interest must be accounted for. Since stopping power is energy dependent it is more accurate to iteratively determine the amount of energy lost in a fraction of the half-life and then re-evaluate the stopping power again at this lower energy.

After computing how much energy was lost by the recoiling nucleus in the material, the original kinetic energy of the nucleus can be found. Finally using conservation laws the kinetic energy of the proton can be calculated and also the CM energy of the decay.

# Chapter 2

## Experiment

### 2.1 Lab Layout

The data used in this thesis was obtained during a  $^{26}\text{P}$   $\beta$ -decay experiment (e10034) which was carried out at the National Superconducting Cyclotron Laboratory (NSCL) at Michigan State University. The Coupled Cyclotron Facility at NSCL is shown in Figure 2.1 [2].

A primary beam of stable  $^{36}\text{Ar}$  was accelerated to about 150 MeV/u by the coupled cyclotrons (K500 and K1200). Then to produce the isotope of interest,  $^{26}\text{P}$ , the accelerated beam was impinged upon a production target of  $^9\text{Be}$  of thickness 1.55 g/cm<sup>2</sup>. The processes of nuclear fragmentation created not only  $^{26}\text{P}$ , but many contaminants as well. To try to purify the beam it next goes through the A1900, a series of tuned magnets which filters out contaminants by magnetic rigidity [15]. This works since each isotope has a different charge/mass ratio and therefore when moving perpendicular to a magnetic field each isotope will start to curve in arcs of different radii. The magnets, and therefore the magnetic field, can be tuned such that the isotope of interest stays in the beam line and others are stopped by physical barriers. This filtering is not perfect since there are isotopes with very similar magnetic rigidities. These isotopes end up being contaminants for the experiment. After the beam passes through the magnets it is further purified by time of flight using a radio-frequency fragment separator [1].

This results in a final beam that is 74% pure with major components being  $^{24}\text{Al}$  and

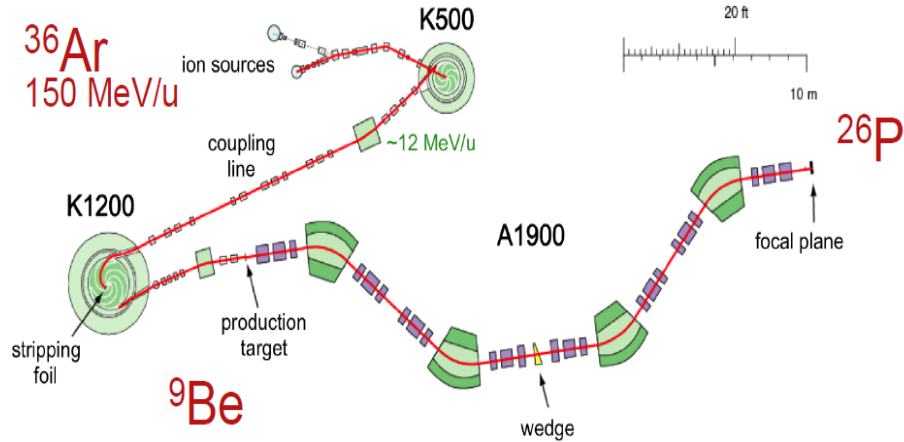


Figure 2.1: The layout of the Coupled Cyclotron Facility at the National Superconducting Laboratory. The beam starts as stable ions that are accelerated by the coupled cyclotrons, the K500 and K1200. Once the stable beam is accelerated it is impinged upon a production target,  ${}^9\text{Be}$  in our case, which creates the isotope of interest ( ${}^{26}\text{P}$ ) along with many other isotopes. This new beam is delivered to the A1900 which helps to purifying the beam using magnets. Next the beam goes to the RFFS which further purifies the beam. Finally the rare isotope beam of interest is sent to the experimental setup.

${}^{22}\text{Na}$ . The particle identification plot in Figure 2.2 shows the energy loss of beam particles versus time of flight. Each concentration of points indicates a different isotope; the points circled in red are the  ${}^{26}\text{P}$  particles of interest.

## 2.2 Detectors

At the end of the beam line, the  ${}^{26}\text{P}$  beam was directed into the S2 vault to the experimental setup. The setup consisted of two detectors: a central detector where the beam was implanted, a Germanium Double Sided Strip Detector (GeDSSD), and a surrounding array of 16 high purity germanium (HPGe) detectors, the Segmented Germanium Array (SeGA). They can be seen in Figure 2.3 (A) and (B) respectively.

The GeDSSD [13] was the implantation system, which is a 1-cm thick planar germanium detector. It is divided by electrodes into 16 segments that are 5 mm wide on the front and

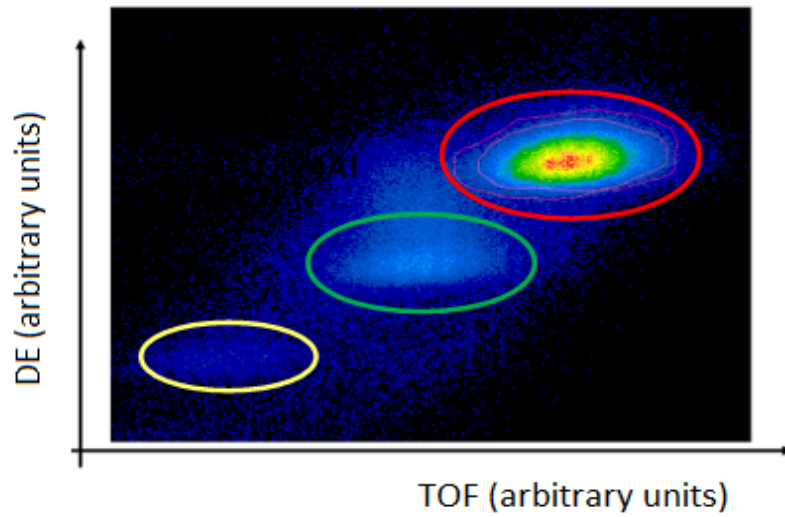


Figure 2.2: The plot shows the energy loss of a particle versus the time of flight (TOF). Each circled concentration of points is a different isotope. The red oval encompasses  $^{26}\text{P}$  particles while the green and yellow encompass the  $^{24}\text{Al}$  and  $^{22}\text{Na}$  particles, respectively.

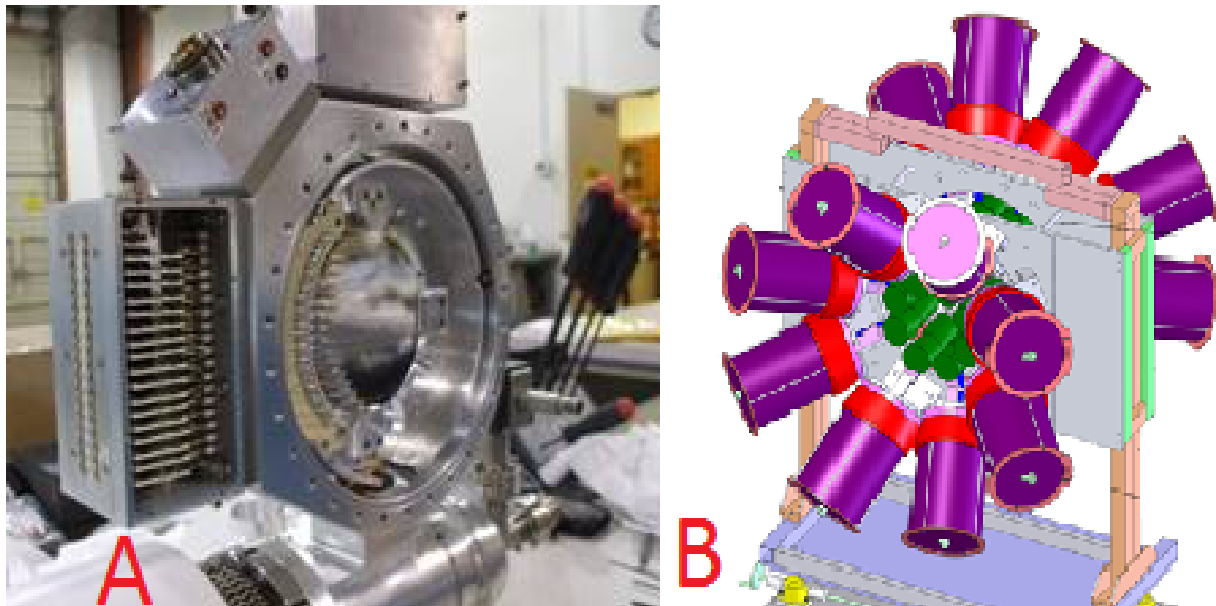


Figure 2.3: (A) The Germanium Double Sided Strip Detector (GeDSSD) with the cryostat open. The secondary beam was implanted into the GeDSSD which detected energy released when a decay occurred. It was surrounded by SeGA in the experiment. (B) A computer aided design (CAD) of the Segmented Germanium Array, SeGA. It is composed of 16 HPGe crystals surrounding the GeDSSD, where the beam was implanted.

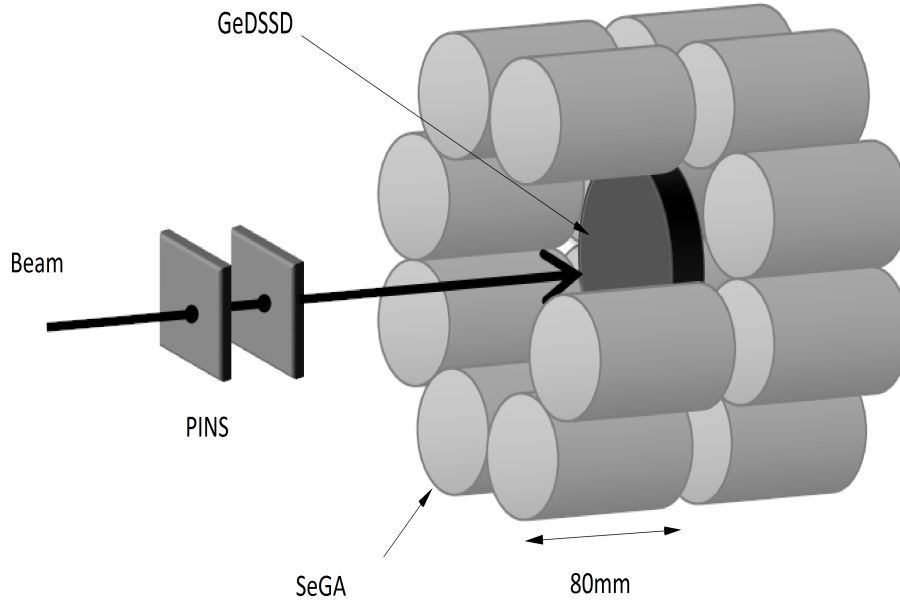


Figure 2.4: This conceptual shows the GeDSSD surrounded by the SeGA Detectors. Figure courtesy of David Pérez-Loureiro

16 similar strips that are orthogonal on the back, providing 256 pixels. The final beam is implanted into the GeDSSD about  $300\ \mu\text{m}$  into the germanium crystal. This is where all the decays of interest would occur.

The  $\gamma$ -ray spectrum from SeGA was energy calibrated using the well known, strongly populated background peaks at  $1460.8\ \text{keV}$  ( $^{40}\text{K}$   $\gamma$  decay) and  $2614.5\ \text{keV}$  ( $^{208}\text{Tl}$   $\gamma$  decay). Efficiency calibrations were performed using three different sources,  $^{154,155}\text{Eu}$  and  $^{60}\text{Co}$ . The sources were placed on the beam axis and data from the decaying sources was collected. Then Monte Carlo simulations of the calibration runs using GEANT 4 [12] were performed and compared to data collected.

Background in the SeGA  $\gamma$ -ray spectra was further reduced by using coincidence gating on signals from  $\beta$ -decays in the GeDSSD. Only when high-gain events were recorded in the GeDSSD would events be accepted by SeGA. The timing gate used was a  $1.2\ \mu\text{s}$  gate. This reduces background since the setup is constantly detecting background radiation, for

example the 1461 keV  $\gamma$  ray from  $^{40}\text{K}$ . The only time that any of the  $^{40}\text{K}$   $\gamma$  rays are included in the final data is when they are detected within the 1.2  $\mu\text{s}$  window surrounding a  $\beta$  or  $\beta$ -delayed proton decay event in the GeDSSD.

# Chapter 3

## Data Analysis and Discussion

After the data was obtained and sorted information about the  $^{26}\text{P}(\beta p \gamma)^{25}\text{Al}$  decay channel to be extracted. The intensity of the population of each of the excited states of  $^{25}\text{Al}$  could be determined, their excitation energy and also information about the center of mass (CM) proton energy could be determined for certain energy levels. Each of these will be discussed in more detail in the following sections.

### 3.1 Gamma-ray Intensities

The peaks determined to be from the  $^{26}\text{P}(\beta p \gamma)^{25}\text{Al}$  decay channel were observed at 452, 493, 844, 930, 944, 1338, 1613, 1776 and 1790 keV and are labeled in Fig. 3.1. The peaks were first identified by searching for peaks at energies previously reported for this decay in Ref. [18]. Peaks at 930 and 1776 keV were new to this decay channel and identified as possible  $^{25}\text{Al}$   $\gamma$ -rays by comparing them to energy differences for known  $^{25}\text{Al}$  level [8]. They correspond to the transitions from excited states at 2720 to 1790 keV and 2720 to 945 keV, respectively, as see in Table 3.2. Coincidence gating was also performed to support the previously known level scheme and the peaks observed in coincidence are reported in Table 3.1.

To fit the peaks and determine the number of events pertaining to each energy the

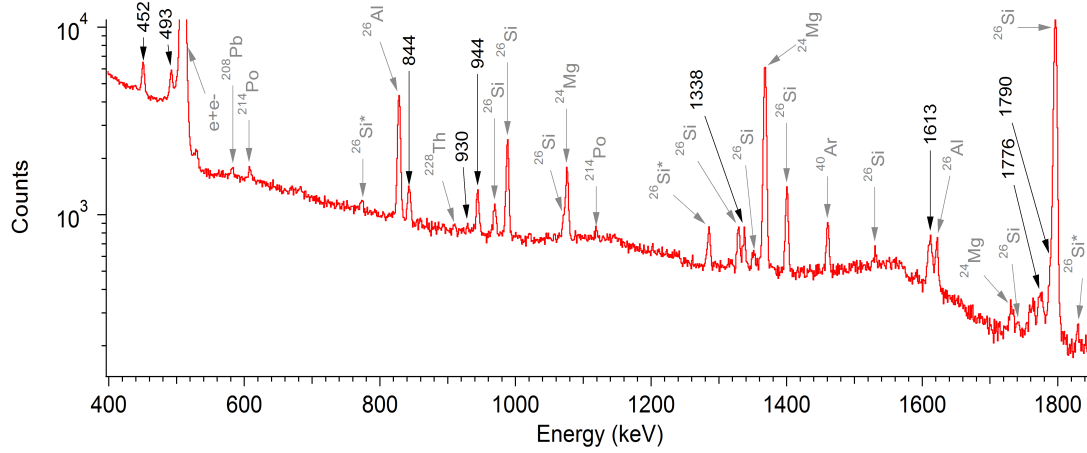


Figure 3.1:  $^{26}\text{P}$   $\beta$ -delayed  $\gamma$ -ray spectrum. All  $\gamma$ -ray peaks attributed to the  $^{26}\text{P}(\beta p \gamma)^{25}\text{Al}$  decay are labeled by their energy in keV (black). Other peaks are labeled by the  $\gamma$ -ray emitting nuclide, with escape peaks denoted by an asterisk (gray). Selected regions are shown in more detail in Fig. 3.7 and Fig. 3.8.

Table 3.1:  $^{26}\text{P}(\beta p \gamma)^{25}\text{Al}$   $\gamma$  rays observed in the present work. The measured  $\gamma$ -ray energies are reported in the 1<sup>st</sup> column with their statistical uncertainties only; the global systematic uncertainty is 0.5 keV. An asterisk denotes  $\gamma$  rays observed for the first time in  $^{26}\text{P}$   $\beta$ -decay. The  $\gamma$ -ray intensity per  $^{26}\text{P}$  decay is reported in the 2<sup>nd</sup> column, where the intensity of the 1613-keV line from [18] was used for normalization. The 3<sup>rd</sup> column lists  $\gamma$  rays observed in coincidence.

Energy (keV)	Intensity (%)	$\gamma$ -ray coincidences
451.9(3)	2.6(3)	493, 844, 930, 1338, 1776
493.1(4)	2.4(3)	452, 844, 1776
843.5(3)	0.8(2)	452, 493, 944
930.4(5)*	0.09(5)	452, 944
944.4(2)	1.2(1)	844, 930, 1776
1338.0(2)	0.8(1)	452
1613.1(3)	2.2(2)	
1775.5(3)*	1.2(1)	452, 493, 944
1790.2(3)	0.8(3)	

response function of SeGA had to be determined. The response function used to fit the peaks in the  $\gamma$ -ray spectrum was an Exponentially modified Gaussian (EMG).

$$f(x) = \frac{A}{2\sigma} \left(1 - \frac{\operatorname{erf}\left(\frac{x-\mu}{\tau} + \frac{\tau}{\sigma}\right)}{\sqrt{2}}\right) \exp\left(\frac{\tau^2}{2\sigma^2} + \frac{x-\mu}{\sigma}\right) \quad (3.1)$$

where  $A$  is the amplitude or integral of the peak,  $x$  represents energy,  $\mu$  represents the center energy,  $\sigma$  is the width and  $\tau$  describes the decay of the exponential component. The reason why the EMG works well as a response function for this spectrum is that it incorporates the Gaussian resolution of the Ge detectors with a low energy tail.

This response function worked well for most of the  $^{25}\text{Al}$  peaks. However, the fitting of the Doppler broadened peaks at 1613 and 1776 keV was more complex. The modeling of these peaks will be discussed in detail in the following sections.

Using well-known  $^{24}\text{Mg}$   $\gamma$ -ray energies from  $\beta$  decay of the  $^{24}\text{Al}$  beam contaminant [9] a  $2^{nd}$ -degree polynomial energy-calibration function was created. The calibration used well-known room background peaks in the  $\gamma$ -ray singles spectrum to verify its accuracy of 0.5 keV. The calibrated  $\gamma$ -ray energies are reported in Table 3.1. The 844 keV peak contains a small contribution from an unresolved  $^{26}\text{P}(\beta\gamma)^{26}\text{Si}$  line at nearly the same energy. In this case, we report the energy of the combined peak. The energies are all consistent with previously reported values when known [8].

Simulations using the GEANT4 Monte-Carlo package [12] were then compared to data taken offline using an absolutely calibrated  $^{154,155}\text{Eu}$  source and the relative intensities of the  $^{24}\text{Mg}$  lines from online data to establish the efficiency as a function of energy of the SeGA detectors. The efficiency curve allowed for the relative intensities of the  $^{25}\text{Al}$   $\gamma$ -rays to be determined. Due to difficulties in determining the total number of  $^{26}\text{P}$   $\beta$ -decays that

occurred in the experiment the absolute intensities were found by normalizing to the 1613 keV  $\gamma$  ray, which is known to have an absolute intensity of  $2.2 \pm 0.2$  % [18] based on the proton feeding of the 1613 keV excited state (Table 3.1). Due to the close proximity of the 844 keV peak and the 842 keV  $^{26}\text{Si}$  peak, its intensity and uncertainty were determined by combining the acquired  $^{26}\text{Si}$  data set with *sd*-shell model calculations [4] to predict, and subtract, the small contribution of  $0.33 \pm 0.17$  % from the  $^{26}\text{P}(\beta\gamma)^{26}\text{Si}$  line.

## 3.2 $\beta p$ Feeding

The feeding of each  $^{25}\text{Al}$  level via  $\beta p$  decay of  $^{26}\text{P}$  was calculated by subtracting the intensity of  $\gamma$ -decay branches feeding it from the intensity of  $\gamma$ -decay branches de-exciting it. For example, as seen in Figure 3.2, the 944 keV excited state is not only fed by proton emission, but also the de-excitation of higher-energy states via the emission of 844 and 1776 keV  $\gamma$  rays. The 944 keV state de-excites via the emission of 493 and 944 keV  $\gamma$  rays. The feeding of the 944 keV state from proton emission is equal to the sum of the intensities of the emitted  $\gamma$  rays minus the sum of the intensities of the  $\gamma$  rays which feed the 944 keV state, all of which can be found in Table 3.1.

Since this experiment was not sensitive to the feeding of the ground state of  $^{25}\text{Al}$  the value of this feeding reported in Table 3.2 and Fig. 3.2 are adopted from [18]. The  $\beta p$  feeding is summarized in Table 3.2 and illustrated in Fig. 3.2. There is good agreement with most of the proton-feeding values from Thomas *et al.* [18]. The only exception is the feeding of the first excited state at 452 keV. Some of the difference can be attributed to their insensitivity to the 2720 keV state, which provides a significant  $\gamma$ -ray feeding of the 452 keV state. The small proton feeding can be explained by the need for an  $\ell \geq 2$  proton to populate this

Table 3.2: The  $^{26}\text{P}(\beta p)$  feeding of  $^{25}\text{Al}$  states found in the present work and previous work [18]. The 452 keV  $\beta$ -feeding is given as an upper limit. Upper limits are calculated at a 95% confidence-level. An asterisk denotes evidence for excited states observed for the first time via this decay channel. The intensities are normalized to the feeding of the 1613-keV level from [18].

$^{25}\text{Al}$ excitation energy (keV)	Proton feeding	
	Present work (%)	Ref [18] (%)
Ground state		27.3 (4)
452	<0.34	2.1 (1)
944	1.6(3)	2.1 (5)
1613	2.2(2)	2.2 (2)
1790	2.3(2)	2.3 (2)
2720*	1.1(1)	

$J^\pi = 1/2^+$  state from the  $J^\pi=(2,3,4)^+$   $^{26}\text{Si}$  states fed by allowed  $^{26}\text{P}$   $\beta$  decay transitions.

### 3.3 Study of Doppler Broadened Peaks

Two peaks in the  $\gamma$ -ray spectrum clearly exhibit Doppler broadening from the recoil due to proton emission. Those peaks are found at 1613 and 1776 keV in the spectrum of Fig. 3.1. The peaks at 1613 keV (Fig. 3.7) and 1776 keV (Fig. 3.8) are from the de-excitation of the 1613 and 2720 keV excited states of  $^{25}\text{Al}$  respectively. Since all of the  $^{25}\text{Al}$  peaks in the spectrum are populated due to  $\beta p$  decay one might expect that Doppler broadening should be observed in all of the  $^{25}\text{Al}$  peaks analyzed in this work. However, due to the proportionality of the Doppler shift on  $\gamma$ -ray energy, we were not sensitive to the Doppler broadening of the lines at 1338 keV and below. Unfortunately, due to the close proximity of the intense 1797 keV  $^{26}\text{Si}$  peak to the 1790 keV  $^{25}\text{Al}$  peak, it was not possible to study the

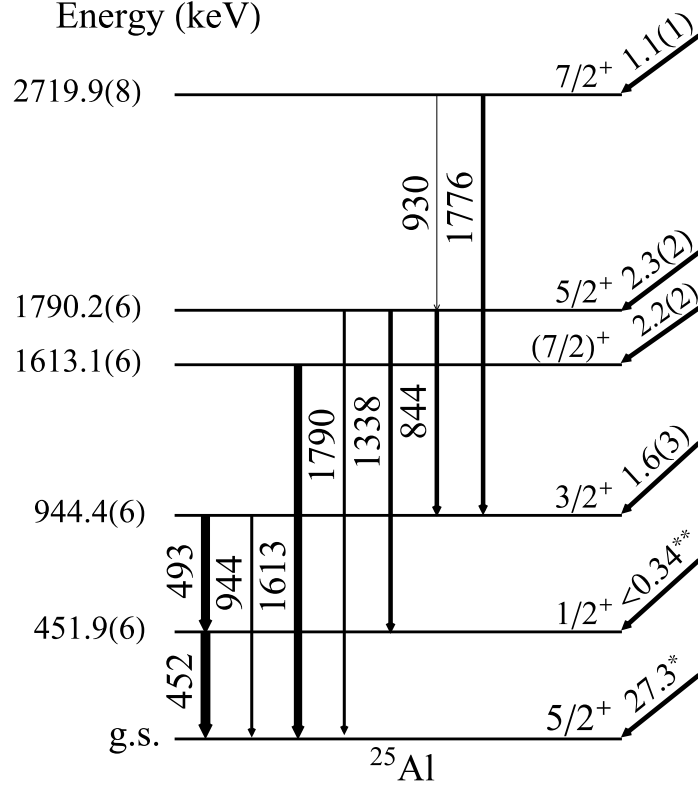


Figure 3.2:  $^{25}\text{Al}$  level scheme from  $^{26}\text{P}(\beta\text{p}\gamma)^{25}\text{Al}$  decay deduced from the present work. The  $\gamma$ -ray transitions observed are denoted by arrows with thicknesses proportional to their intensities and labeled by  $\gamma$ -ray energy in keV. The  $\beta\text{p}$  feeding of the different excited states is depicted by the arrows on the right, which are labeled by the intensities. The single asterisk denotes a value adopted from [18]. The double asterisks denotes the upper limit of the  $\beta$ -feeding of the 452 keV state at the 95% confidence level.

broadening of the 1790-keV peak precisely. The physical process creating broadened peaks in our  $\gamma$ -ray spectrum was discussed in detail in the Introduction. Fitting these peaks requires several steps. If the broadened peak is from a state fed by a previously known proton energy, then the kinetic energy of the recoiling nucleus that emits the  $\gamma$ -ray can be calculated. For example, consider only the 2288 keV CM proton energy which feeds the 1613 keV excited state in  $^{25}\text{Al}$ . One can find the initial velocity of the excited  $^{25}\text{Al}$  nucleus by conservation of momentum and energy as seen below.

$$E = \frac{1}{2}m_p v_p^2 + \frac{1}{2}m_{Al} v_{Al}^2 = 2288\text{keV} \quad (3.2)$$

$$p = m_p v_p + m_{Al} v_{Al} \quad (3.3)$$

$$E = \frac{1}{2}m_p \left(\frac{m_{Al} v_{Al}}{m_p}\right)^2 + \frac{1}{2}m_{Al} v_{Al}^2 = 2288\text{keV} \quad (3.4)$$

$$v_{Al} = 8.2 \cdot 10^5 \frac{m}{s} \quad (3.5)$$

Where  $m$  is mass,  $v$  is velocity and subscripts  $p$  and  $Al$  stand for proton and  $^{25}\text{Al}$  nuclei respectively. Assuming that the  $\gamma$  decay occurred in free space this would be the velocity of the nucleus at the time of  $\gamma$  decay and the velocity can be used directly to calculate the Doppler broadening.

$$E'_{(max)} = \left(\frac{c}{c - v_{al}}\right)E_{\gamma} = 1616\text{keV} \quad (3.6)$$

where  $E'_{(max)}$  is the maximum shifted energy that can be detected due to Doppler shift and  $E_{\gamma}$  is the original unshifted energy of the  $\gamma$  ray.  $E'_{(max)}$  can either be the maximum or minimum possible Doppler shifted energy depending on the sign of  $v_{al}$ . We can find the difference in these two energies, 3 keV, which will be used as the parameter which determines how broad our peak of interest is [10]. For these broadened peaks, a model using a boxcar function convoluted discretely with the EMG response function is employed. A simplified version can be seen in Equation 3.7.

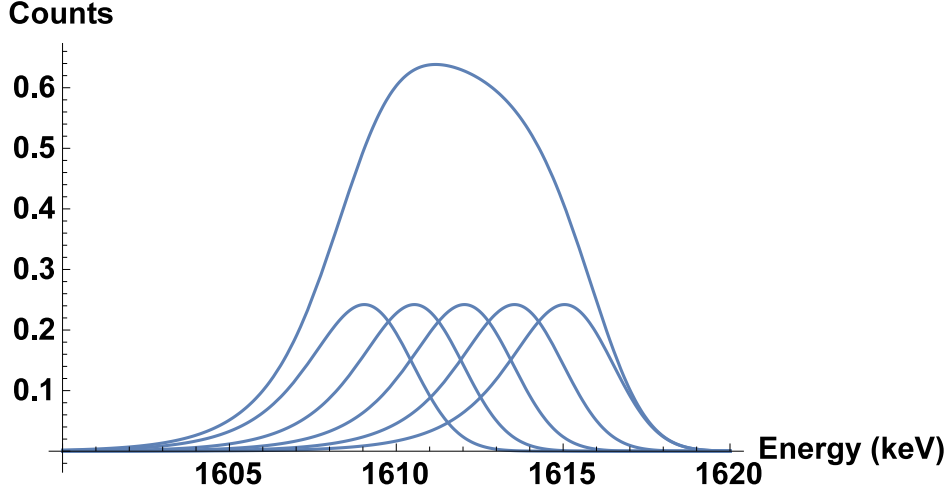


Figure 3.3: This plot shows how the boxcar function convoluted EMGs produce a broadened peak. In this example  $\mu= 1613$  keV,  $\sigma = 1.54$ ,  $\tau = 1.2$ ,  $\lambda = 3$  keV and the amplitude of the smaller peaks are set to one.

$$\begin{aligned}
f(x) = & \frac{A}{2\sigma} \left(1 - \frac{\operatorname{erf}\left(\frac{x-\mu+\lambda}{\tau} + \frac{\tau}{\sigma}\right)}{\sqrt{2}}\right) \exp\left(\frac{\tau^2}{2\sigma^2} + \frac{x-\mu+\lambda}{\sigma}\right) \\
& \frac{A}{2\sigma} \left(1 - \frac{\operatorname{erf}\left(\frac{x-\mu+0.5\lambda}{\tau} + \frac{\tau}{\sigma}\right)}{\sqrt{2}}\right) \exp\left(\frac{\tau^2}{2\sigma^2} + \frac{x-\mu+0.5\lambda}{\sigma}\right) \\
& \frac{A}{2\sigma} \left(1 - \frac{\operatorname{erf}\left(\frac{x-\mu}{\tau} + \frac{\tau}{\sigma}\right)}{\sqrt{2}}\right) \exp\left(\frac{\tau^2}{2\sigma^2} + \frac{x-\mu}{\sigma}\right) \\
& \frac{A}{2\sigma} \left(1 - \frac{\operatorname{erf}\left(\frac{x-\mu-0.5\lambda}{\tau} + \frac{\tau}{\sigma}\right)}{\sqrt{2}}\right) \exp\left(\frac{\tau^2}{2\sigma^2} + \frac{x-\mu-0.5\lambda}{\sigma}\right) \\
& \frac{A}{2\sigma} \left(1 - \frac{\operatorname{erf}\left(\frac{x-\mu-\lambda}{\tau} + \frac{\tau}{\sigma}\right)}{\sqrt{2}}\right) \exp\left(\frac{\tau^2}{2\sigma^2} + \frac{x-\mu-\lambda}{\sigma}\right)
\end{aligned} \tag{3.7}$$

where  $A$  is the amplitude,  $\mu$  is the central energy,  $\tau$  is the decay constant,  $\sigma$  is the width of the Gaussian and  $\lambda$  is the “stretch parameter”, which is the difference in  $E'_{(max)}$  and  $E_\gamma$  calculated above. Using the parameters relevant for the 1613 keV peak, we can plot the simplified version of the peak and all of its contributions.

However, in the actual case of the 1613 keV  $\gamma$ -ray peak, it is known that two different CM energy protons feed the 1613 keV level in  $^{25}\text{Al}$  [18] as seen in Fig.3.4. Therefore,

the function used in modeling this peak requires a linear combination of two boxcar EMG functions. These boxcar functions are centered at the same energy and have the same  $\tau$  and  $\sigma$  parameters. The difference in the two boxcar functions is that one of the functions has an amplitude that is twice the other [18] and that their  $\lambda$  stretch parameter is different.

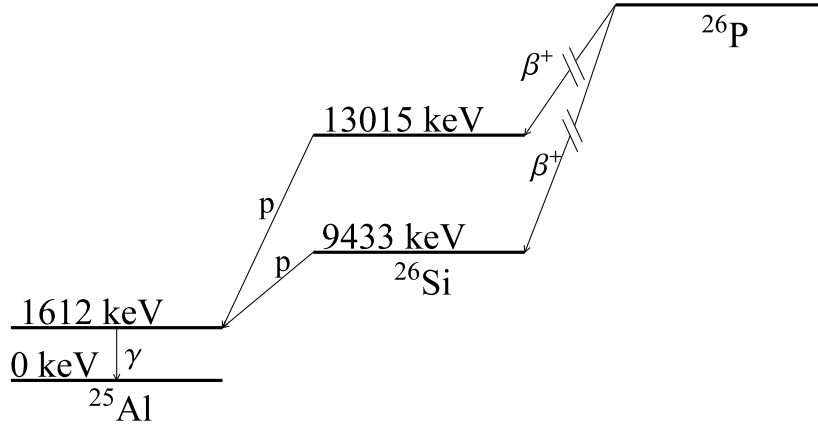


Figure 3.4: The previously known decay scheme for the  $^{26}\text{P}$   $\beta$ -delayed proton emission to the 1613 keV excited state of  $^{25}\text{Al}$  [18]. Two proton-unbound  $^{26}\text{Si}$  states feed the 1613 keV  $^{25}\text{Al}$  excited state, causing two different  $^{25}\text{Al}$  recoil velocities following proton emission.

Another way that our simplified case is not appropriate for our actual data is that the decay does not occur in free space. It instead occurs in the GeDSSD, which is germanium and, therefore, the recoiling nucleus will begin to slow down as soon as it is emitted. It is necessary to incorporate the half life of the excited state of  $^{25}\text{Al}$  that the  $\gamma$ -ray is emitted from and it is used along with the stopping power of the material in which the nucleus is moving to determine the velocity of the  $^{25}\text{Al}$  at the time of  $\gamma$  decay. As shown previously, once the velocity at the time of  $\gamma$ -ray emission is determined along with the expected energy of the  $\gamma$  ray the maximum possible  $\gamma$ -ray energy that can be detected due to Doppler broadening can be calculated.

The final piece of information missing from our simplified case is the fact that not all of the decays occurs exactly at the half-life. Instead that is the time by which 50% of decays are

expected to have occurred. To more accurately depict this in our model we expanded what was one boxcar function for each proton into 5 boxcar functions each of which represent a different time interval between proton emission and  $\gamma$ -ray emission. We discretized the decay,

$$N(t) = N_0 \frac{1}{2} \frac{t}{t_{\frac{1}{2}}} \quad (3.8)$$

where  $N(t)$  is the current number of particle that have not yet decayed,  $N_0$  are the number of original particles that can decay,  $t_{\frac{1}{2}}$  is the half-life and  $t$  is time.

Using the known value of  $\tau$ , the times at which 10, 30, 50, 70 and 90% of the decays are expected to have occurred were calculated. Each of these discrete times was used to represent 20% of the decays, providing five relationships between the initial velocity and the velocity at the time of  $\gamma$ -ray emission through the stopping power. Figure 3.5 shows the exponential decay for a particle with a theoretical half-life of 10 fs and initial count of 100 particles. Black lines divide the decay where 20%, 40%, 60% and 80% of the particles have decayed. For each C. M. proton energy a boxcar step function was created corresponding to each of the five times such that they had equal integrals and stretched in unison. The stopping power was treated by utilizing SRIM tables generated for  $^{25}\text{Al}$  ions in germanium [20]. For the 1776-keV case the stopping power was treated iteratively in 25 fs steps to account for its energy dependence due to its relatively long half-life of 201(14) fs [9]. Figure 3.6 shows how the shape of the peak changes when evaluated at different times along the decay for the 1776 keV  $\gamma$ -ray case. It illustrates why it is important to evaluate the Doppler shift at more than just the half-life of the decay. There are more accurate ways to treat the half-life and stopping power; however, this discrete treatment was sufficiently accurate

considering the statistical uncertainties in the spectrum and the absolute uncertainty in the stopping power, which was approximated to be 10% based on the scatter in the experimental data plots from SRIM for aluminum ions in germanium.

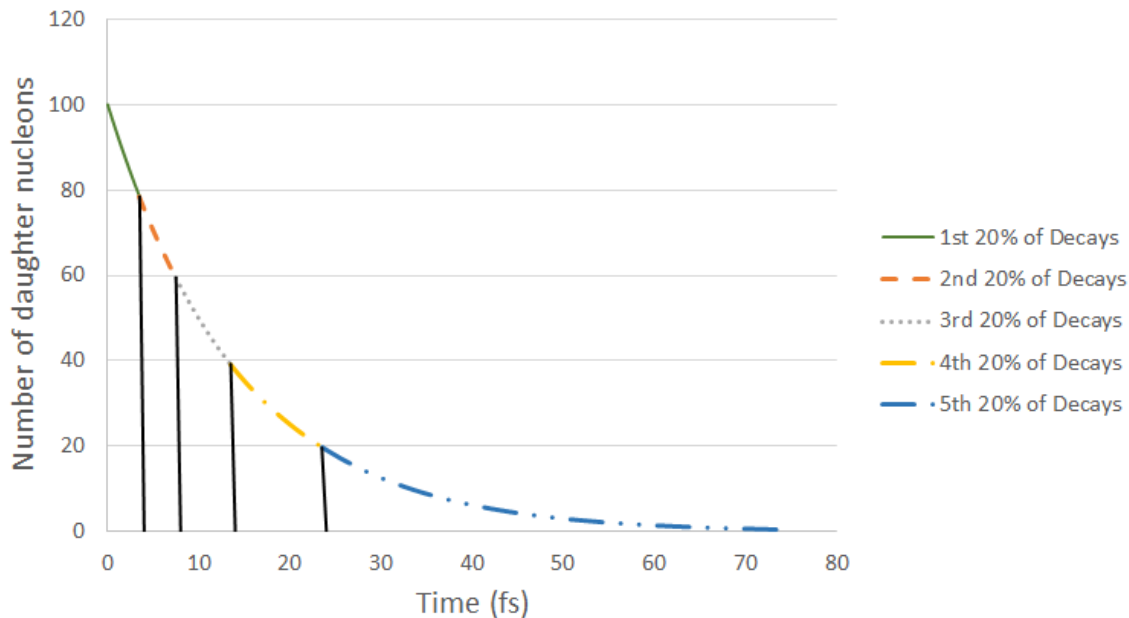


Figure 3.5: The decay of a theoretical particle with initially 100 daughter particles and a half-life of 10 fs is shown above. For the analysis the decay curve was divided into five sections like shown above. The time used to represent the Doppler broadening of the first 20% of decaying particles would be the time at which it is expected for 10% of the particle to have decayed. The other fifths are evaluated in the same manner.

### 3.4 1613 keV

The C. M. energies and relative intensities for the protons that feed the 1613 keV excited state are well known [18]. With this previously reported information we could test the Doppler broadening method by adopting these energies along with the known lifetime to constrain the fit (Fig. 3.7).

The Compton background in the 1613-keV region was continuous and flat and was there-

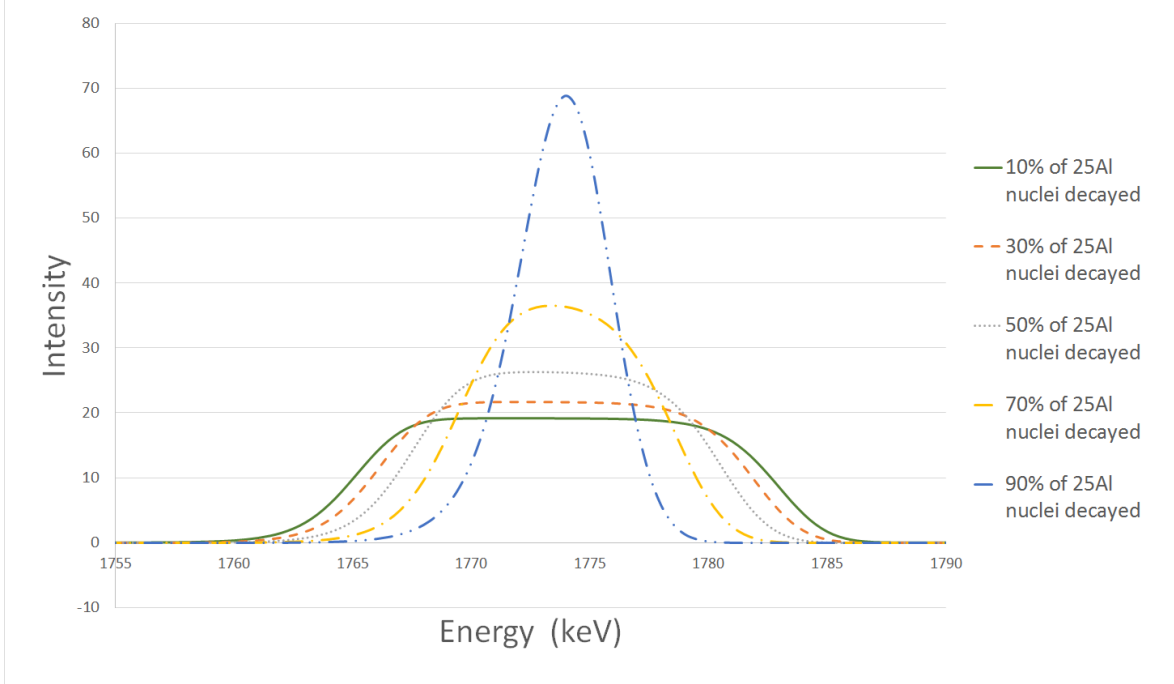


Figure 3.6: The components of the final shape of the 1776 keV  $\gamma$ -ray peak are shown above. Each peak has the same number of counts, but the spreads due to Doppler broadening are different due to evaluating them at the time here 10% (green solid line), 30% (orange dashed line), 50% (grey dotted line), 70% (yellow dot-dashed line) and 90% (blue double dot-dashed line) of the particles have decayed. The response function used for this figure is Gaussian for simplicity.

fore modeled with a straight line. The neighboring contaminant  $^{26}\text{Al}$  peak at 1622.26(3) keV (from  $^{26}\text{Si}$   $\beta$  decay) [7] was not broadened and could be modeled with a simple EMG with the amplitude and the centroid as free parameters. Another background peak is in the region at 1611.807(11) keV [7] and is the result of the well-known  $\beta$  decay of  $^{25}\text{Al}$  to excited states of  $^{25}\text{Mg}$ . Since the absolute intensity of this  $\gamma$  ray is known it was possible to fix the intensity of the corresponding peak to be 0.112 times that of the 1613 keV peak. This confirms that the overlap of the weak  $^{25}\text{Mg}$   $\gamma$ -ray line to the  $^{25}\text{Al}$   $\gamma$ -ray line does not contribute significantly to the broadening of the 1613 keV peak.

Initially the 1613 keV peak was treated as if there was no Doppler broadening by using the same response function used to model the other peaks in the spectrum. This yielded

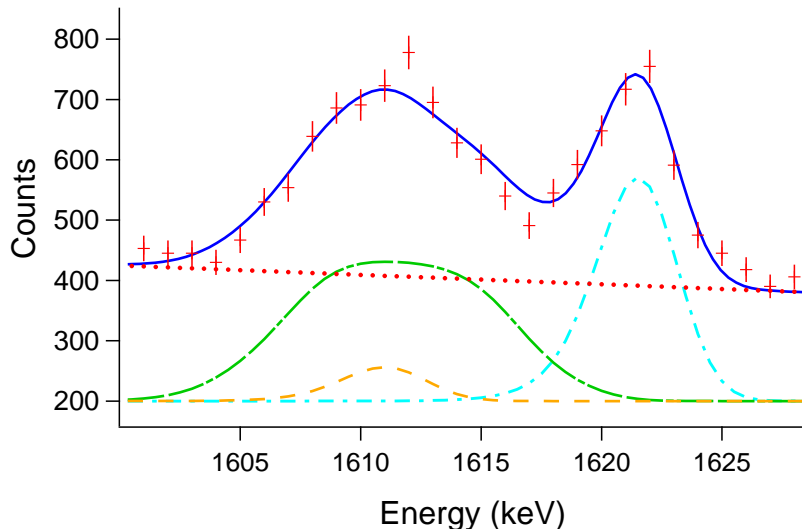


Figure 3.7:  $^{26}\text{P}$   $\beta$ -delayed  $\gamma$ -ray spectrum in the region of the  $^{25}\text{Al}$  peak at 1613 keV. The peak at 1613 keV is broader than the neighboring  $^{26}\text{Al}$  peak at 1622 keV. The solid blue line is the overall fit including Doppler broadening and the red dotted line represents the Compton scattering background. Below the data and fit, the individual peak components are shown. The 1611 keV  $^{25}\text{Mg}$ , 1613 keV  $^{25}\text{Al}$  and 1622 keV  $^{26}\text{Al}$   $\gamma$ -ray lines are represented by the green dot-double-dashed, gold dashed and light blue dot-dashed lines, respectively.

a high  $\chi^2$  per degree of freedom of 138/27 corresponding to a p-value of 0.0001. It was, therefore, clear that the assumption that the 1613 keV peak should be modeled with the same EMG response function without broadening is incorrect.

Next Doppler broadening due to the proton emission was incorporated into the model, as described previously. There are two different excited states above the proton threshold in  $^{26}\text{Si}$  that emit protons populating the 1613 keV excited state of  $^{25}\text{Al}$ , which undergoes a  $\gamma$ -ray transition to the ground state [18]. The C. M. energies of the two protons are 2288(3) keV and 5893(4) keV and they have a relative intensity of  $I_{2288}/I_{5893} = 2.0$  (Fig. 3.4) [18]. There was substantial improvement of the fit after including Doppler broadening with these known values (Fig. 3.7) and it is reflected in the improvement in the  $\chi^2$  per degree of freedom to 31.5/27 corresponding to a p-value of 0.25. This confirmed the Doppler broadening of this line as well as the accuracy of the Doppler broadening analysis technique [10]. We were

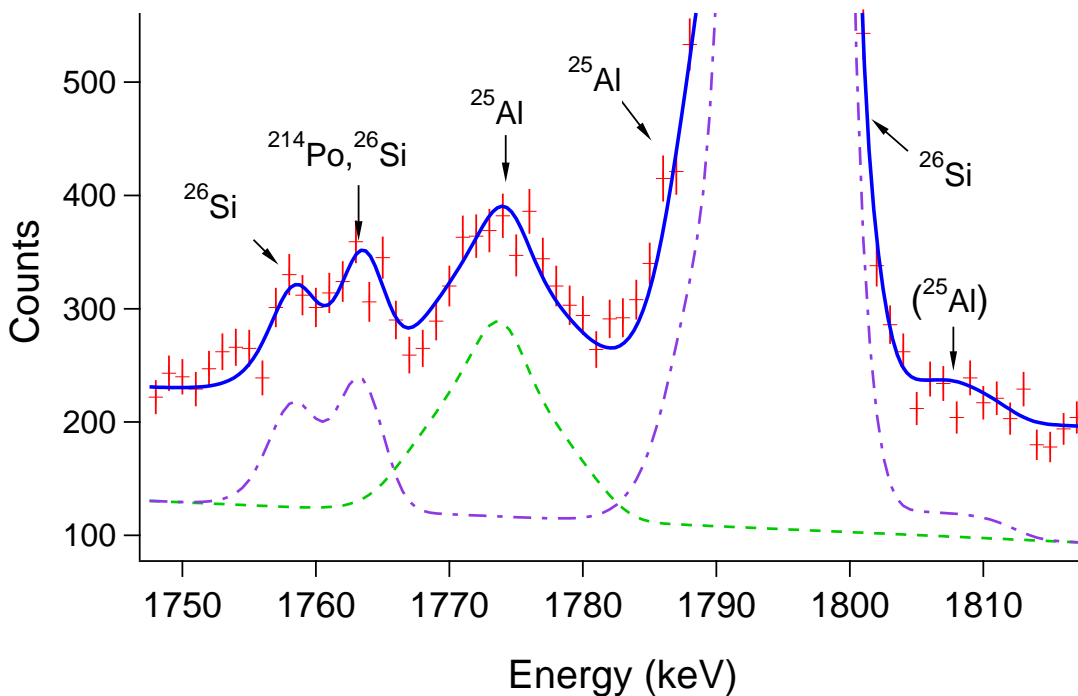


Figure 3.8: (Color online)  $^{26}\text{P}$   $\beta$ -delayed  $\gamma$ -ray spectrum (red crosses) in the region of the 1776- and 1790-keV peaks with fit (blue solid line). The dashed green line shows the contribution of the Doppler broadened 1776-keV peak to the overall fit. The dot-dashed purple line shows the contributions of all other peaks. The small excess near 1810 keV could not be confirmed to be from  $^{25}\text{Al}$ .

further encouraged to utilize this method to try to extract the CM energy from the 1776 keV peak which has no known proton CM energy.

### 3.5 1776 keV

The 1776 keV  $\gamma$ -ray transition from the 2720 keV excited state of  $^{25}\text{Al}$  was observed for the first time in  $^{26}\text{P}$   $\beta$  decay (Fig. 3.8) [17]. Since it has never been observed via this decay mechanism the C. M. proton energy feeding the 2720 keV excited state was unknown. This allowed us to extract this new information using the application of the Doppler broadening method.

As in the 1613 keV region, the continuous Compton scattering component of the back-

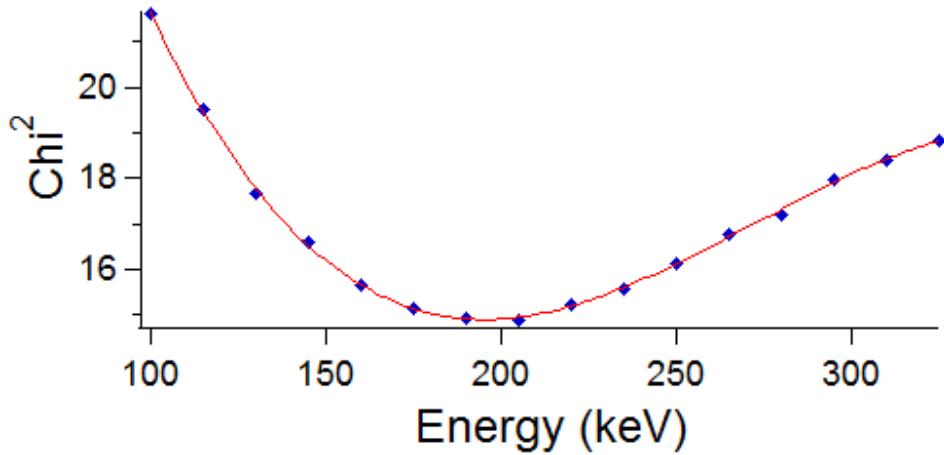


Figure 3.9: The blue dots show the  $\chi^2$  value for each of the initial  $^{25}\text{Al}$  kinetic energy tested. The blue line shows the quadratic fit line that was used to determine the energy with the minimum  $\chi^2$ . The minimum was found to be at  $195^{+41}_{-50}$  (*stat.*)  $\pm 18$  (*syst.*) keV

ground was modeled to be linear. To provide an accurate representation of the background underneath the 1776-keV peak it was necessary to include the other peaks in the region in the fit function. The 1790 keV  $^{25}\text{Al}$  peak on the shoulder of the strong 1797-keV  $^{26}\text{Si}$  line was modeled to be Doppler broadened; its shape was constrained using the three known proton energies [18] feeding it, their ratios and the known half life of the 1790 keV excited state [8].

To find the CM energy for the 1776 keV peak while incorporating stopping power and the half-life we used hypothesized initial  $^{25}\text{Al}$  recoil energies and varied them in the fit from 100 to 325 keV in 15 keV steps. The best fit and  $\chi^2$  value were found for each of these energies.

Plotting the CM energies versus the  $\chi^2$  value of the fit resulted in an optimal  $^{25}\text{Al}$  initial kinetic energy of  $195^{+41}_{-50}$  (*stat.*)  $\pm 18$  (*syst.*) keV based on the minimum value of  $\chi^2$  as seen in Fig. 3.9. Using conservation of energy and momentum the corresponding C. M. proton energy was found to be  $5.1 \pm 1.0$  (*stat.*)  $\pm 0.6$  (*syst.*) MeV corresponding

Table 3.3: Sources of uncertainty in the  $5.1 \pm 1.0$  (*stat.*)  $\pm 0.6$  (*syst.*) MeV  $^{26}\text{P}$   $\beta$ -delayed proton C. M. energy feeding the 2.72 MeV  $^{25}\text{Al}$  state.

Source of uncertainty	Uncertainty (MeV)
statistics	1.0
response function	0.3
stopping power	0.5
background	0.1

to a proton-emitting  $^{26}\text{Si}$  level at an excitation energy of  $13.3 \pm 1.0$  (*stat.*)  $\pm 0.7$  (*syst.*) MeV. Systematic uncertainties for the proton energy were derived from the uncertainties in the shape parameters of the response function, uncertainties in the stopping power, and uncertainties in the background. A summary of the uncertainties can be found in Table 3.3, which shows that the stopping power contributes the dominant systematic uncertainty. The only proton unbound state of  $^{26}\text{Si}$  that is consistent with our measured proton energy is the isobaric analog state (IAS) of  $^{26}\text{P}$  at 13.015(4) MeV (the only known excited state above 10.8 MeV), which is also known to be strongly populated in  $^{26}\text{P}$   $\beta$  decay [18].

# Chapter 4

## Conclusion and outlook

While the method demonstrated in the present work is not quite of similar accuracy to direct techniques which measure the proton CM energies from  $\beta$ -delayed proton- $\gamma$  decay, it is much more difficult to measure  $\beta$ -delayed neutron CM energies. The present method may prove to be very useful to the measurement of neutron energies since it does not require the emitted nucleon to be charged. There have been proposals to further refine the way  $\gamma$ -ray data is collected which will be a next potential step for this method.

To obtain more precise results in the future it is possible that Crystal diffraction spectrometer (CDS) measurements will be the key [5]. It has already been proposed to use CDS at ISOL@MYRRHA (Isotope separator on-line) in Belgium to study  $\beta$ -delayed neutron emission [19]. The advantages to using CDS is that the resolution of  $\gamma$  ray energies is much better than that of HPGe crystal detectors. The down side it that the detector for CDS necessarily has a low acceptance, giving it a much smaller solid angle, and therefore a much lower efficiency. One way to combat this is to use very intense beams (like those produced at ISOL@MYRRHA or, potentially, FRIB) and to have long experimental run times to allow for the sufficient collection of statistics.

The great resolution of CDS would allow for the CM energies from higher mass cases to be determined. It will also yield more precise energies for lower mass cases. While this may not be a competitive method to obtain  $\beta$ -delayed proton CM energies, it is significant to the detection of the CM energies of  $\beta$ -delayed neutrons, due to their neutral nature.

To conclude, this was the first observation of the radiative Doppler broadening from  $\beta$ -delayed proton- $\gamma$  decay, and it was also the highest mass ( $A=25$ ) for which Doppler broadening has been observed in any  $\beta$ -delayed nucleon- $\gamma$  decay. Since there was not one but two peaks with obvious Doppler broadening this not only allowed us to test the technique presented in [10] with a case with a known CM proton energy, but also apply the technique to determine a previously unknown CM proton energy. Absolute intensities of 8 different energy  $\gamma$  rays from  $^{26}\text{P}(\beta p\gamma)^{25}\text{Al}$  were determined as was the  $\beta$  feeding of 5  $^{25}\text{Al}$  excited states from the same decay. The present results have been published in Ref. [17].

# Bibliography

- [1] D. Bazin et al. “Radio Frequency Fragment Separator at NSCL”. In: *Nucl. Instrum. Methods A* 606 (July 2009), pp. 314–319. DOI: 10.1016/j.nima.2009.05.100.
- [2] M. B. Bennett et al. “Classical-Nova Contribution to the Milky Way’s Al26 Abundance: Exit Channel of the Key Al25(p, $\gamma$ )Si26 Resonance”. In: *Phys. Rev. Lett.* 111.23 (2013), p. 232503. DOI: 10.1103/PhysRevLett.111.232503.
- [3] M. J. Borge et al. “Elucidating halo structure by  $\beta$  decay:  $\beta\gamma$  from the  $^{11}\text{Li}$  decay”. In: 55 (Jan. 1997), p. 8. DOI: 10.1103/PhysRevC.55.R8.
- [4] B. A. Brown. private communication. 2013.
- [5] SCK CEN. *MYRRHA: Multi-purpose hybrid research reactor for high-tech applications*. 2016. URL: <http://myrrha.sckcen.be/en> (visited on 03/25/2016).
- [6] S. Y. F. Chu, L. P. Ekström, and R. B. Firestone.
- [7] P. M. Endt. “Supplement to Energy Levels of A=21-44 Nuclei (vii)”. In: *Nucl. Phys.* A633 (Apr. 1998). [www.nndc.bnl.gov/ensdf](http://www.nndc.bnl.gov/ensdf), pp. 1–220.
- [8] R. B. Firestone. In: *Nucl. Data Sheets* 110 (July 2009), p. 1691. DOI: 10.1016/S0168-583X(03)00570-6.

- [9] R. B. Firestone. “Nuclear Data Sheets for  $A = 24$ ”. In: *Nucl. Data Sheets* 108 (Nov. 2007), p. 2319. DOI: 10.1016/j.nds.2007.10.001.
- [10] H. O. U. Fynbo. “Doppler broadened  $\gamma$ -lines from exotic nuclei”. In: *Nucl. Instrum. Methods Phys. Res. B* 207 (2003), p. 275. DOI: 10.1016/S0168-583X(03)00570-6.
- [11] H. O. U. Fynbo et al. “New information on the  $\beta$ -decay of  $^{11}\text{Li}$  from Doppler broadened  $\gamma$  lines”. In: *Nucl. Phys. A* 736 (May 2004), pp. 39–54. DOI: 10.1016/j.nuclphysa.2004.02.020.
- [12] Geant4 Collaboration and S. Agostinelli *et al.* (Geant4 Collaboration). “Geant4-a simulation toolkit”. In: *Nucl. Instrum. and Methods A* 506 (July 2003), pp. 250–303.
- [13] N. Larson et al. “High efficiency beta-decay spectroscopy using a planar germanium double-sided strip detector”. In: *Nucl. Instrum. Methods Phys. Res. A* 727 (2013), p. 59. DOI: 10.1016/j.nima.2013.06.027.
- [14] C. M. Mattoon et al. “Line-shape analysis of Doppler-broadened  $\gamma$  lines following the  $\beta$  decay of  $\text{Li}11$ ”. In: 80.3, 034318 (Sept. 2009), p. 034318. DOI: 10.1103/PhysRevC.80.034318.
- [15] D. J. Morrissey et al. “Commissioning the A1900 projectile fragment separator”. In: *Nucl. Instrum. Methods B* 204 (May 2003), pp. 90–96. DOI: 10.1016/S0168-583X(02)01895-5.
- [16] F. Sarazin et al. “Halo neutrons and the  $\beta$  decay of  $^{11}\text{Li}$ ”. In: 70.3, 031302(R) (Sept. 2004), 031302(R). DOI: 10.1103/PhysRevC.70.031302.
- [17] S. B. Schwartz et al. “Observation of Doppler broadening in  $\beta$ -delayed proton- $\gamma$  decay”. In: *Phys. Rev. C* 92 (3 2015), p. 031302. DOI: 10.1103/PhysRevC.92.031302. URL: <http://link.aps.org/doi/10.1103/PhysRevC.92.031302>.

- [18] J.-C. Thomas et al. “Beta-decay properties of  $^{25}\text{Si}$  and  $^{26}\text{P}$ ”. In: *Eur. Phys. J. A* 21 (Sept. 2004), pp. 419–435. DOI: 10.1140/epja/i2003-10218-8.
- [19] P. C. Womble et al. *The Doppler-broadening of Gamma-ray Spectra in Neutron-Based Explosives Detection Systems*. 2009. URL: [http://www-pub.iaea.org/MTCD/publications/PDF/P1433\\_CD/datasets/abstracts/sm\\_en-16.html](http://www-pub.iaea.org/MTCD/publications/PDF/P1433_CD/datasets/abstracts/sm_en-16.html).
- [20] J. F. Ziegler and J. P. Biersack. “The Stopping and Range of Ions in Matter”. In: *Treatise on Heavy-Ion Science*, by Bromley, D. Allan, ISBN 978-1-4615-8105-5. Springer-Verlag US, 1985, p. 93. Ed. by D. A. Bromley. 1985, p. 93. DOI: 10.1007/978-1-4615-8103-1\_3.